Quasiwetting on spherical solid surfaces by oil-water-amphiphile mixtures

C. García-Alcántara and C. Varea
Universidad Nacional Atónoma de México, Apartado Postal 20-364, 01000 México D.R., Mexico
(Received 20 April 2006; published 14 September 2006)

We study the wetting behavior on spherical walls by ternary mixtures of oil, water, and an amphiphile. We use the Ginzburg-Landau free energy with a single order parameter and find that there are different stable structures of the interface and that a quasiwetting transition is the mechanism involved in the transition among them. We calculate these wetting transitions for two sets of parameters in the bulk free energy which are known to show microemulsion behavior. The surface transitions are thin-thick first-order transitions (continuous transitions are absent), and the phase diagram in surface parameter space is constructed. For the first set of bulk parameters water, oil, and a microemulsion coexist, and we study the first-order transition where the oil phase wets the wall-microemulsion interface and its behavior as the radius of the wall becomes large. Therefore, we recover the known wetting transitions on a planar wall. In the second set of bulk parameters only water and oil coexist, and for some sizes of the solid wall, the oil phase wets the wall-water interface, and the phase behavior is extremely rich. We obtain a coexistence of four surface phases or two triple points followed by three lines of first-order transitions which end at three critical points depending on the radius of the surface. When there are micellar metastable solutions in bulk, the behavior of the thickness of the wetting layer of the oil phase as the radius of the spherical wall gets larger is nonmonotonic. We associate this behavior with the intrinsic micelle structure due to the spontaneous curvature of the model.

DOI: 10.1103/PhysRevE.74.031603 PACS number(s): 68.08.Bc, 47.57.jb, 68.05.Gh

I. INTRODUCTION

The properties of curved interfaces have proved to be crucial for the understanding of equilibrium phases that have mesoscopic structures, like those that occur in solutions of amphiphiles with otherwise immiscible solvents, as in water and oil microemulsions. There is a great interest in these mixtures because of their properties and the many technological applications [1,2], like in pharmaceutical industry, oil recovery, etc. In many applications a particle is introduced inside the microemulsion and the result is colloidal arrays so that the study of the wetting properties of a particle inside these complex fluids, and its control, is of importance.

The main property of these mixtures is the self-assembly into a variety of complicated structures. In these mixtures there are regions of oil and water separated by monolayers of surfactant, which can fill the space in several interesting arrangements. The microemulsion is one of these and it is formed by oil-rich and water-rich bicontinuous regions separated by amphiphiles. They can also form water/oil and oil/water micelles with amphiphile monolayers at their surfaces. On the other hand, there are lamellar phases that conform a one-dimensional stacking of amphiphile sheets filled by water or oil. For these systems, it is thought that the interfacial energy is the main contribution that differentiates the diverse structures, and Helfrich has proposed an interfacial free energy that includes interfacial tension in addition to interfacial bending and spontaneous curvature terms. Several authors have studied these systems with Ginzburg-Landau models, and they have calculated the phase diagrams in bulk [3] and the elastic properties of the interfaces [4]. These same elastic properties were studied by Robledo and Varea [5,6], with the same model, where also the stability of the amphiphilic spherical interfaces has been studied; there, the stability region of (metastable) micellar phases was found. Furthermore, these authors find solutions of the Euler-Lagrange equations that are unstable and correspond to nucleation.

There are some studies of the wetting behavior of these mixtures on planar interfaces. These include the wetting on the oil-water interface by a microemulsion phase. This transition appears due to the amphiphile properties and the approximation to the tricritical points [7]; other authors found that the lamellar phase wets a planar wall-oil interface [8]. Finally, Clarysse and Boulter studied the wetting on a solid-wall–microemulsion interface [9]; these authors used the Ginzburg-Landau model in the derivation of an effective interface Hamiltonian for an amphiphilic system and found that the oil phase wets this interface and this unbinding depends on the surface parameters. In some cases the wetting is preceded by a thin-thick transition leading to the presence of additional critical points in the surface phase diagram. Also there are studies, with lattice models, on the wetting behavior in systems with amphiphiles near a planar surface [10]. In addition to these the confinement of these complex fluids [11] has been studied in Monte Carlo simulations. There has also been experimental work on the properties of the planar surface correlations in microemulsions where surface-induced layering was found [12] and the surface correlation is significantly larger than its bulk analog [13].

The quasiwetting transition on spherical substrates has been studied in simple fluids. Several theories have been used to model these phenomena [14–17], and the wetting of silica particles by lutidine in water has been confirmed experimentally [18]. These transitions are thin-thick transitions, and when constructing the full phase diagram it is found that there is a particular behavior with respect to planar transitions like the appearance of other types of critical points [16]. As far as we know there is no study of wetting by complex fluids like mixtures of oil, water, and an amphiphile on this curved surface.

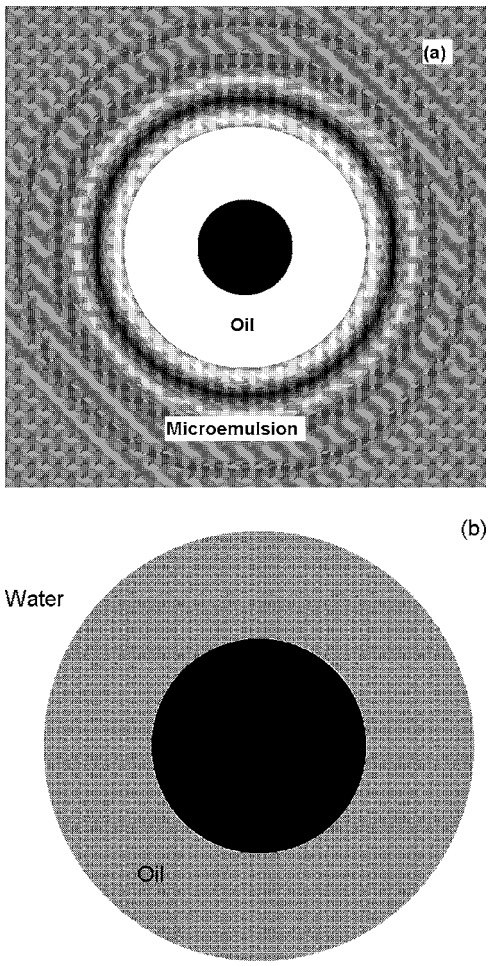

FIG. 1. Schematic representation of the two kinds of quasiwetting studied. In (a) the oil phase wets the interface between the solid (in black) and microemulsion phases. In (b) the oil wets the interface between the solid and water interface.

In this work we calculate the wetting transitions on the spherical wall by a water-oil-amphiphile mixture; see Fig. 1. We find the density profiles, and we calculate the phase diagrams. We also introduce the interface potential as an additional tool to study the quasiwetting transitions. We study two types of interfaces; one of them is the wall-microemulsion interface where the microemulsion is stable and has a structure factor with decaying oscillations. Here the three phases (water, oil, and microemulsion) are in coexistence and the local part of the free energy is symmetric with respect to the concentrations of water and oil in bulk. Here we look for quasiwetting transitions where the oil phase wets the wall-microemulsion interface. Since the water phase has a smaller order parameter than both oil or microemulsion, effectively in this case there is only the competition of oil and microemulsion phases near the wall. We compare these surface transitions with the same interface in a planar wall and find that, in the limit of infinite radius of the wall, we recover the first-order wetting transitions.

The other case is the wall-water-phase interface. Here the uniform "microemulsion" phase is metastable and the local part of the water-oil free energy is asymmetric. Here we find that the intrinsic micelle structure due to the spontaneous curvature produces transitions where the wetting layer is a nonmonotonic function of the radius of the spherical surface. The resulting phase diagram is extremely rich due to the existence of three different microscopic structures at the wall-water interface.

The paper is organized as follows: In Sec. II we introduce the model used and some of its properties. In Sec. III we study some of the properties of the wall-microemulsion interface and find quasiwetting transitions where the oil phase quasiwets the solid-microemulsion interface. In Sec. IV we show the rich behavior of the phase diagram for a solid-water interface when the surface chemical potential favors the formation of the oil-phase in contact with a solid spherical particle. In Sec. V we summarize and discuss our results.

II. GINZBURG-LANDAU MODEL

We consider a sphere of radius R immersed in a water-oil-amphiphile mixture. The grand potential density functional with a single order parameter, $\phi=\phi(\mathbf{r})$, can be written as $\Omega[\phi]=\Omega_b[\phi]+\Omega_s[\phi]$, where

$$\Omega_b[\phi]=\int\left\{f(\phi)+\frac{1}{2}A(\phi)(\nabla\phi)^2-\frac{1}{4}B(\phi)(\nabla^2\phi)^2-\mu\phi\right\}d^3\mathbf{r} \tag{1}$$

and

$$\Omega_s=\int\{\mu_s\phi_s+\omega_s\phi_s^2+g_s(\nabla\phi_s)^2\}d^2\mathbf{r}, \tag{2}$$

where μ_s is the wall potential and ω_s measures the difference between the surface interactions and the bulk interactions. g_s is related to a local chemical potential of the amphiphile at the wall, $f(\phi)$ is the free-energy density of the uniform system, and μ is the chemical potential. The quantities $A(\phi)$ and $B(\phi)$ are, respectively, proportional to the second and fourth moments of the direct pair correlation function (see Fig. 2). $\phi(\mathbf{r})$ is the order parameter and can be thought to represent the local difference in the concentration of the two solvents. The free-energy density $f(\phi)$ can be chosen to have the following piecewise parabolic three-parabola-model (TPM) form:

$$f=\begin{cases}\lambda_w(\phi-\phi_{bw})^2, & \phi<\phi_2,\\ \lambda_a\phi^2+f_0, & \phi_2<\phi<\phi_1,\\ \lambda_o(\phi-\phi_{bo})^2, & \phi_1<\phi.\end{cases} \tag{3}$$

Here the two minima at ϕ_{bw} and ϕ_{bo} represent the uniform equilibrium phases when $\mu=0$ of solvents w and o, respectively. The height of the central minima at $\phi=0$ is controlled by the parameter f_0, and decreasing its value has an effect suggestive of the addition of amphiphile to the mixture, and when $f_0=0$ the minimum at $\phi=0$ corresponds to an equilibrium solution of the two solvents and a phase rich in amphiphile. We consider that A has the stepwise form

$$A=\begin{cases}A_w>0, & \phi<\phi_2,\\ A_a<0, & \phi_2<\phi<\phi_1,\\ A_o>0, & \phi_1<\phi.\end{cases} \tag{4}$$

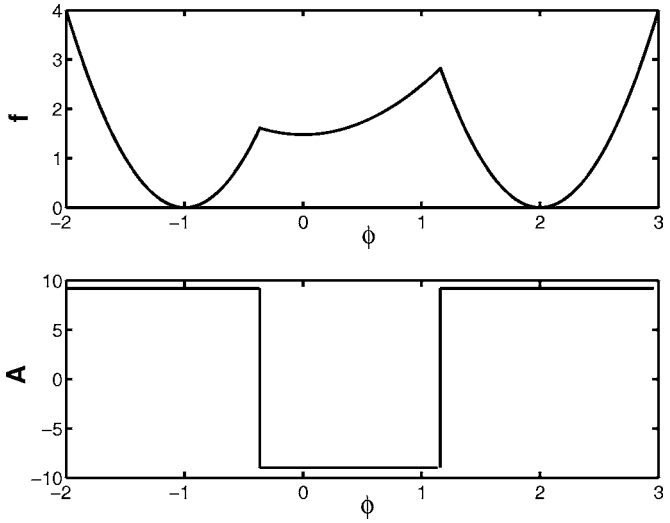

FIG. 2. The functions $f(\phi)$ and $A(\phi)$ with the values $f_0=1.48$, $\phi_{bw}=-1.0$, $\phi_{bo}=2.0$, $\lambda_o=\lambda_w=4.0$, $\lambda_a=1.0$, $A_o=A_w=9.2$, $A_a=-9.0$, and $B=-4.0$. In $f(\phi)$ the middle phase is metastable.

The negative value of A_a generates a peak in the model's structure factor at nonzero wave vector [19], and B is a constant independent of ϕ that needs to be negative for stability.

The Euler-Lagrange equation associated with Eq. (1) is

$$\frac{\delta\Omega}{\delta\phi}=\frac{df}{d\phi}-\mu-A\nabla^2(\phi(\mathbf{r}))-\frac{1}{2}\frac{dA}{d\phi}|\nabla\phi|^2-\frac{1}{2}B\nabla^4\phi=0. \tag{5}$$

Since f is piecewise parabolic and A is piecewise constant, the differential equation is piecewise linear and the solution of the homogeneous part of the equation is of the form

$$\phi(r)=\sum_i C_{\alpha i}\frac{1}{r}\exp(k_{\alpha i}r), \tag{6}$$

where $\alpha=w,a,o$, represent the water phase, amphiphile (microemulsion) phase, and oil phase, respectively. The decay constants $k_{\alpha i}$ are the roots of the characteristic equation

$$Bk_{\alpha i}^4+2A_\alpha k_{\alpha i}^2-4\lambda_\alpha=0. \tag{7}$$

These functions are continuous with continuous first and second derivatives. The coefficients $C_{\alpha i}$ are obtained with the appropriate boundary conditions on R_1 and R_2, where $\phi(R_1)=\phi_1$ and $\phi(R_2)=\phi_2$:

$$B\left(\left.\frac{d^3\phi_w}{dr^3}\right|_{R_2}-\left.\frac{d^3\phi_a}{dr^3}\right|_{R_2}\right)+(A_w-A_a)\left.\frac{d\phi}{dr}\right|_{R_2}=0, \tag{8}$$

$$B\left(\left.\frac{d^3\phi_a}{dr^3}\right|_{R_1}-\left.\frac{d^3\phi_o}{dr^3}\right|_{R_1}\right)+(A_a-A_o)\left.\frac{d\phi}{dr}\right|_{R_1}=0 \tag{9}$$

and the boundary conditions on the wall

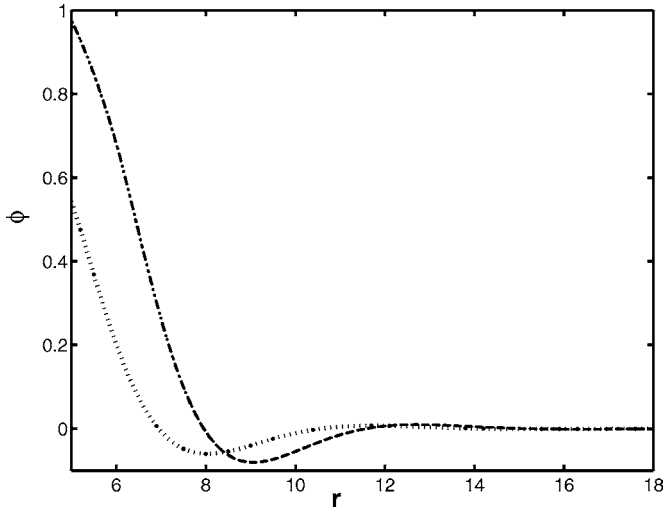

FIG. 3. Two spherical profiles of the wall-microemulsion interface, calculated in the TPM model. The bulk parameters are in the text, $R=5.0$ and $g_s=1.0$. The dash-dotted line corresponds to the surface parameters $\mu_s=-2.85$ and $\omega_s=0.25$. For the dotted line, $\mu_s=-1.0$ and $\omega_s=0.4$.

$$\mu_s+2\omega_s\phi(R)+\left.\frac{d\phi}{dr}\right|_R\left\{\frac{B}{R^2}-A(\phi(R))\right\}-\frac{B}{2}\left.\frac{d^3\phi}{dr^3}\right|_R-\frac{B}{R}\left.\frac{d^2\phi}{dr^2}\right|_R=0, \tag{10}$$

$$\left.\frac{d\phi}{dr}\right|_R\left\{2g_s+\frac{B}{R}\right\}+\frac{B}{2}\left.\frac{d^2\phi}{dr^2}\right|_R=0. \tag{11}$$

III. WALL-MICROEMULSION INTERFACE

We study this interface in the case where there is oil-water symmetry where $\phi_{bo}=-\phi_{bw}=1$, $\lambda_w=\lambda_o$ and $A_w=A_o$. To fix the bulk parameters we review the phase diagram for the model in bulk [3]. This phase diagram has three regions where the oil-rich and water-rich phases are in equilibrium and where the microemulsion and lamellar phases are stable. If we choose $f_0=0$, $B=-4.0$, $A_a=-2$, $\lambda_w=4.0$, $\lambda_a=1.0$, and $A_w=9.0$, the system corresponds to a region where the correlation function in the uniform microemulsion phase has an oscillatory behavior and is in equilibrium with the water phase and the oil phase. To study the wetting properties, we consider the case when the wall prefers the oil phase, then $\mu_s<0$.

We can have two different classes of spherical profiles. The first resides in the middle parabola and corresponds to a wall-microemulsion interface. This profile can be written in the form

$$\phi(r)=\frac{B_1}{r}e^{-k_{a1}r}+\frac{B_2}{r}e^{-k_{a2}r},\quad R<r<\infty, \tag{12}$$

where the coefficients B_1 and B_2 are calculated using the boundary conditions on the wall. We call this the thin 1 profile, for reasons that will be explained later.

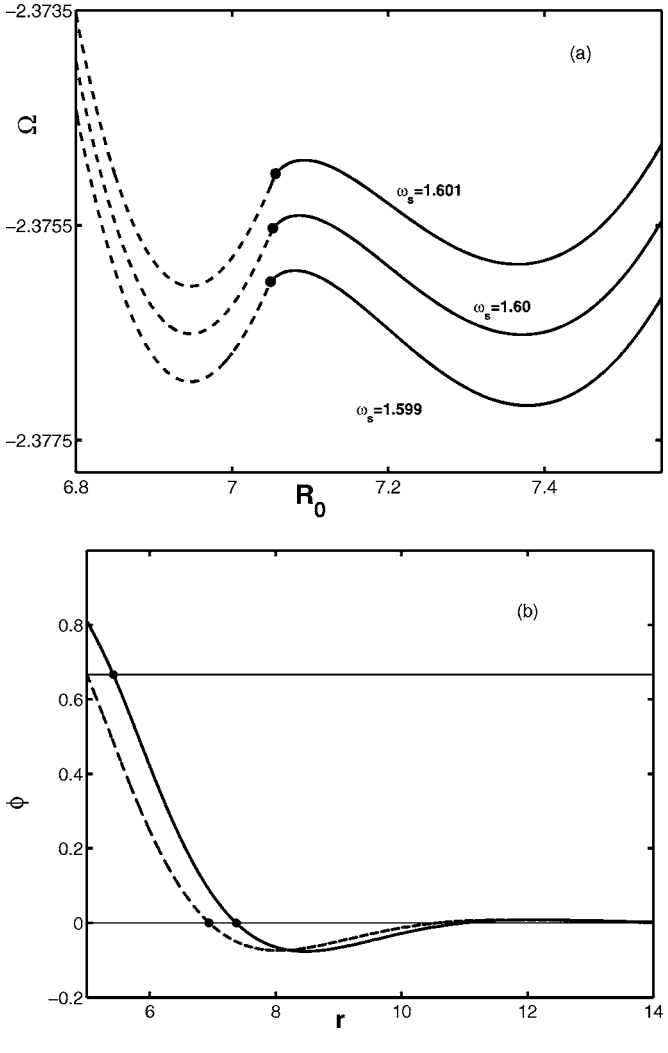

FIG. 4. In (a) we plot three interface potentials close to the first-order transition (thin-thick transition). Here $g_s=1.0$, $\mu_s=-4.9781$, and $R=5.0$; the values of ω_s are in the figure. The transition occurs at $\omega_s=1.6$ in the middle curve where the two minima have the same energy. The dashed line is constructed with profiles of the type thin 2 and the solid line with the thick profiles. In (b) we show the equilibrium profiles at coexistence.

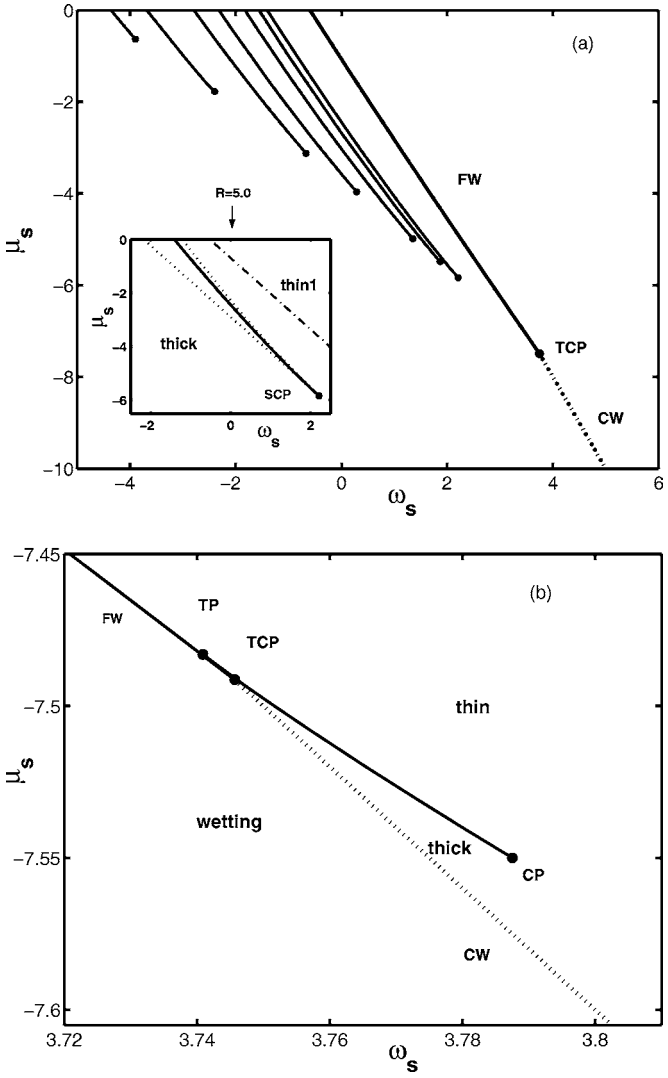

FIG. 5. In (a), phase diagrams for different values of R showing their convergence to a single curve for large R. In the inset we show, as dotted lines, the limits of metastability of the two phases and the dash-dotted line marks the limit of thin1 interfaces. The curve to the right of the diagram corresponds to $R\to\infty$. In (b) detail of the surface phase diagram for the planar interface for the ternary mixture in contact with a planar surface, reproduced from the work in Ref. [9]. There are first-order (FW) and continuous transitions (CW), shown as a dotted line. The two boundaries are separated by a tricritical point (TCP). The thin-thick transitions end at a surface critical point (CP). When the two first-order transitions meet we find a triple point (TP).

The other profile corresponds to the wall-oil-microemulsion interface; this thick profile crosses the point R_1 where $\phi(R_1)=\phi_1=2/3$. Then the profile may be written in the form

$$\phi(r)=\begin{cases}\displaystyle\sum_{i=1}^{4}\frac{A_i}{r}e^{k_{oi}(r-R)}+\phi_{bo}, & R<r<R_1,\\ \displaystyle\frac{B_1}{r}e^{-k_{a1}(r-R_1)}+\frac{B_2}{r}e^{-k_{a2}(r-R_1)}, & R_1<r<\infty,\end{cases}\tag{13}$$

where the intervals $R<r<R_1$ and $R_1<r<\infty$, correspond, respectively, to the regions rich in oil ($\phi>\phi_1$) and rich in amphiphile ($\phi_2<\phi<\phi_1$). The determination of the coefficients A_i and B_i follows from the boundary conditions and the condition that ϕ together with its first and second derivative must be continuous in R_1. The third derivative follows Eq. (9). At this point we can calculate the phase behavior in this system.

In different regions of the parameter space (ω_s-μ_s) we obtain different oscillatory profiles with Eqs. (12) and (13); see Fig. 3. When these are introduced in Eq. (1) we calculate the equilibrium free energy. We then compare the energy between these two states and in principle find the wetting transitions. However, as we follow a line for μ_s constant and decrease the value of ω_s, in parameter space, the value of $\phi(R)$ for the thin 1 profile in the solution of the Euler-

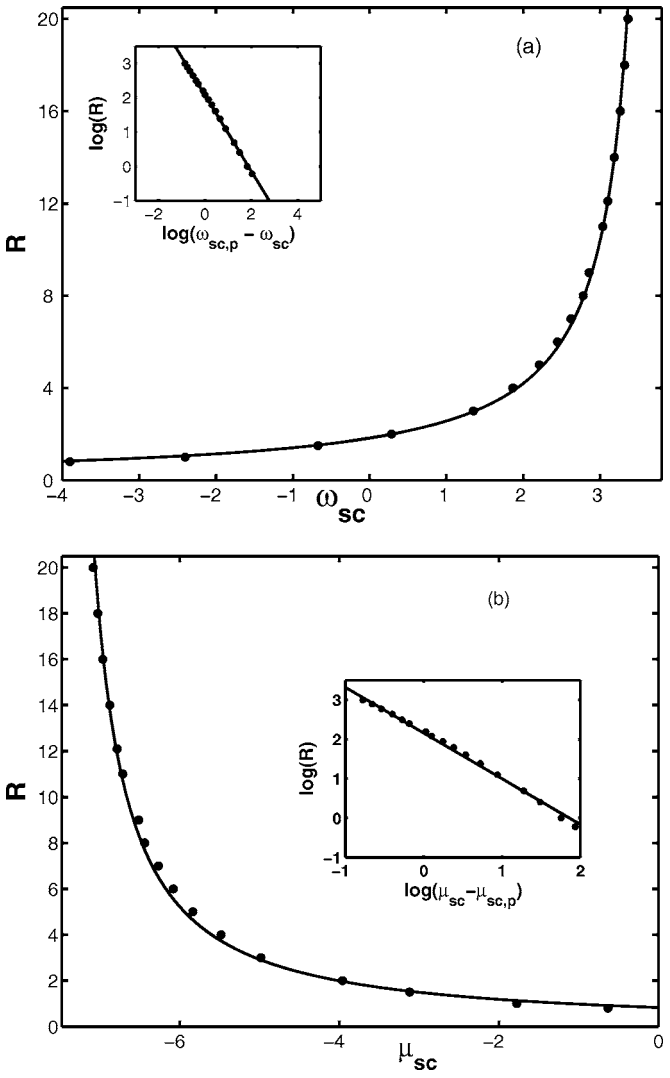

FIG. 6. In (a) we show the fitting of the data corresponding to the behavior of the critical point in the $(R-\omega_{sc})$ space for an spherical wall of radius R. The inset corresponds to the log-log plot where we obtain the fitting parameters used in the solid fitting curve. In (b) we show the same behavior in the $(R-\mu_{sc})$ space. The equivalent analysis assuming that the critical points go to the tricritical point gives a larger error in the fit.

Lagrange equation reaches the value ϕ_1 at the spherical surface. At this point this solution ceases to exist. Moreover, in this region, there are no solutions of the form of Eq. (13) because they are beyond their metastability region. The spinodal point is such that $\phi(R)=\phi_1$. Right at this point, the function A is discontinuous and thus undetermined in Eq. (10). Since the limits of metastability for both the thin 1 and thick profiles satisfy $\phi(R)=\phi_1$, it is only natural to seek profiles with a value of $\phi(R)=\phi_1+\varepsilon$; in the limit $\varepsilon\to 0$, these do not have to satisfy Eq. (9) and give the lowest free energy. These profiles are local minima of the energy and therefore could be more stable than the profile in Eq. (13) in the regions where both exist. It has been argued [9] that some restriction should be included such that $R=R_1-\delta$, where δ is some microscopic length scale over which the profile can vary sufficiently to satisfy the wall constraints. Instead, the

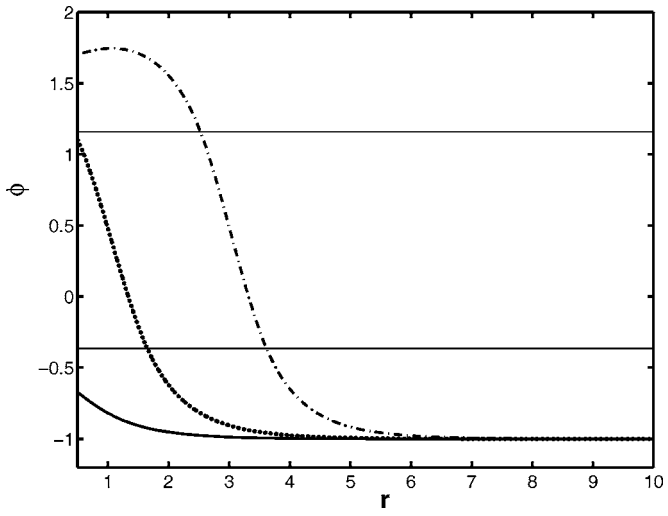

FIG. 7. Spherical equilibrium profiles for the solid-water interface. The dash-dotted curve corresponds to the quasiwetting of oil in the solid-water interface; in the dotted curve the microemulsion is in contact with the wall and in the solid curve there is a simple profile where water is in contact with the wall. The surface parameters are $\mu_s=-10.0$, $\omega_s=6.0$, and $g_s=6.0$. The value of R is $R=0.5$. These three states are not in coexistence.

solutions that we seek satisfy the wall constraints but do not satisfy the discontinuity of the third derivative at $R=R_1$. We view this situation as a consequence of the discontinuities of the model that permit local minima in regions where absolute minima are absent, and we call this profile the thin 2 phase. Notice that in the limit $\varepsilon\to 0$ the value of $A(\phi)$ in the boundary, Eq. (10), acquires the value A_o, while $A(\phi)$ is A_a in the same equation for the thin 1 profile.

This will become clear when we calculate the wetting transition by means of an effective potential. We follow the suggestion used by Varea and Robledo [6] and calculate the profiles that minimize an effective potential per unit of area of the following form:

$$\frac{\Omega(R_0)}{4\pi} = \int_R^\infty \left\{ f(\phi(r)) + \frac{1}{2}A\left(\frac{d\phi}{dr}\right)^2 - \frac{1}{4}B\left(\frac{1}{r^2}\frac{d}{dr}r^2\frac{d\phi}{dr}(r)\right)^2 + V\delta(r-R_0)\phi(r)\right\} r^2 dr + \Omega_s. \tag{14}$$

That is, we introduce an external potential that locates the profile at some distance R_0 from the origin and where

$$\Omega_s = R^2\left\{\mu_s\phi_s + \omega_s\phi_s^2 + g_s\left(\frac{d\phi}{dr}\right)_s^2\right\}. \tag{15}$$

V is a constant that determines the value of the profile at the radius R_0, and $\delta(r-R_0)$ is the Dirac delta function. In practice, we fix the value $[\phi(R_0)=0]$ of the profile at $r=R_0$ from which the strength of the external potential V may be obtained. The Euler-Lagrange equations for this effective potential give rise to the following profiles:

$$\phi(r,R_0)=\begin{cases}\sum_{i=1}^{4}\frac{A_i}{r}e^{k_{oi}r}+\phi_{bo}, & R<r<R_1,\\ \sum_{i=1}^{4}\frac{B_i}{r}e^{k_{ai}(r-R_0)}, & R_1<r<R_0,\\ \frac{C_1}{r}e^{-k_{a1}(r-R_0)}+\frac{C_2}{r}e^{-k_{a2}(r-R_0)}, & R_0<r<\infty,\end{cases} \tag{16}$$

where the profile has two crossing points. The other profile is calculated from the middle parabola

$$\phi(r,R_0)=\begin{cases}\sum_{i=1}^{4}\frac{B_i}{r}e^{k_{ai}(r-R_0)}, & R<r<R_0,\\ \frac{C_1}{r}e^{-k_{a1}(r-R_0)}+\frac{C_2}{r}e^{-k_{a2}(r-R_0)}, & R_0<r<\infty.\end{cases} \tag{17}$$

The constants A, B, and C and the radius R_1 are determined by the same boundary conditions at R_1 as before. At R_0 the profiles are continuous with first and second derivatives continuous and, as mentioned before, we fix $\phi(R_0)=0$. The resulting interface potential has three regions; one of them is constructed with the profile of the Eq. (16). This region ends when $R_1=R$. At this point we use the profiles resulting from Eq. (16); dropping the boundary condition on the discontinuity of the third derivative and fixing $\phi(R,R_0)=\phi_1$, the third region is constructed from Eq. (17). Constructing the effective grand potential is a useful tool because now we can assure that the extremal solutions obtained from the Euler-Lagrange equations are not maxima of the grand potential. Then the wetting transitions are obtained from the iterative calculations and we use this potential to check their stability. In Fig. 4(a) the two minima at the same height correspond to the two coexisting phases and the third region of the effective potential, which is out of scale, is a decreasing function of R_0 and joins smoothly with that of region two. Finally two coexisting profiles are in Fig. 4(b). These correspond to the thick phase and the thin 2 phase, respectively. As we increase R along a μ_s=const trajectory, over the two phase equilibrium lines, the thickness of the quasiwetting layer increases logarithmically.

As we vary the radius of the surface, we see that there exists a surface of critical points (SCP) where the two phases become equal, as shown in Fig. 5(a). In the inset we show the metastable boundaries where some states still exist as well as the limit of validity of the thin 1 profiles.

We have also reproduced the phase diagram in a planar wall [9] in Fig. 5(b). As done before [9], we analyze it and see several characteristics. There is a triple point from which two lines of the first-order transition split. In one branch, the first-order wetting transitions become continuous at a tricritical point. In the other line there are thin-thick transitions, associated with oscillations on the interface potential; these begin at the triple point and end at a surface critical point. Comparing with the wetting transitions on the sphere we find that, in this system, there are no lines of continuous wetting

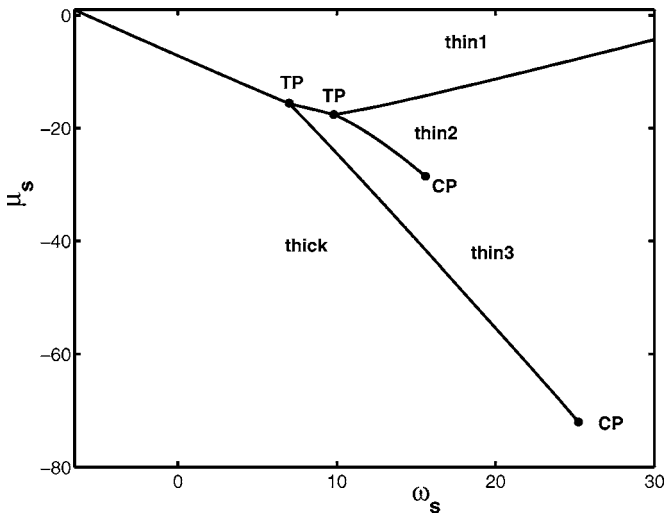

FIG. 8. Phase diagram showing four regions of stability in the (ω_s, μ_s) plane for $R=0.6$ and $g_s=6.0$. There are two triple points (TP), three lines of coexistence, and three critical points (CP). The critical point for the thin-1–thin-2 interface is too far to be seen in this figure.

[Fig. 5(a)] and in the sphere there are only first-order phase transitions associated with a thin-thick transitions that terminate at a surface critical point. We do not find other transitions of the type thin-thick near these critical points, for the radii used. As the radius of the surface grows, the planar wall first-order transitions are recovered; this is shown in Fig. 5(a), where the surface critical points tend to the planar critical point. This behavior is observed in Fig. 6, where in Fig. 6(a) we find, in the inset, that $\log(R)$ vs $\log(\omega_{sc,p}-\omega_{sc})$ is linear and of the form $\log(R)=c+d\log(\omega_{sc,p}-\omega_{sc})$ where the fitted value of d is $d=-1.1\pm0.1$. Here, ω_{scp} is the value of ω_s at the planar critical point. In the same manner in Fig. 6(b) $\log(R)=a+b\log(\mu_{sc}-\mu_{sc,p})$, where $\mu_{sc,p}$ is the value of the critical point in the $\lim R\to\infty$. The fitted value of b is $b=-1.16\pm0.2$. We then conclude that the behavior of R vs $\mu_{sc}-\mu_{scp}$ and R vs $\omega_{sc,p}-\omega_{sc}$ is logarithmic. We have extended our calculations up to $R=100$ (for larger values of R our matrix methods become singular) and made a careful analysis along the thin-thick transition of the spherical interface. We have not found any evidence of the existence of a third thick phase that is present at the triple point in the planar interface. This is not surprising since the minimum of the effective potential for the thick phase is very shallow for $R\to\infty$.

IV. WALL-WATER-PHASE INTERFACE

The second set of bulk parameter values correspond to those shown in Fig. 2 and we have two uniform stable solutions in coexistence: the water and oil phases. Here we are interested in the solid-wall-water interface when the surface chemical potential μ_s favors the oil interface. In the same way as before we can build the general TPM profile and study the wetting transitions on this interface. The bulk parameters used are $\phi_{bo}=2$, $\phi_{bw}=-1$, $\lambda_w=\lambda_o$, and $A_w=A_o$. We

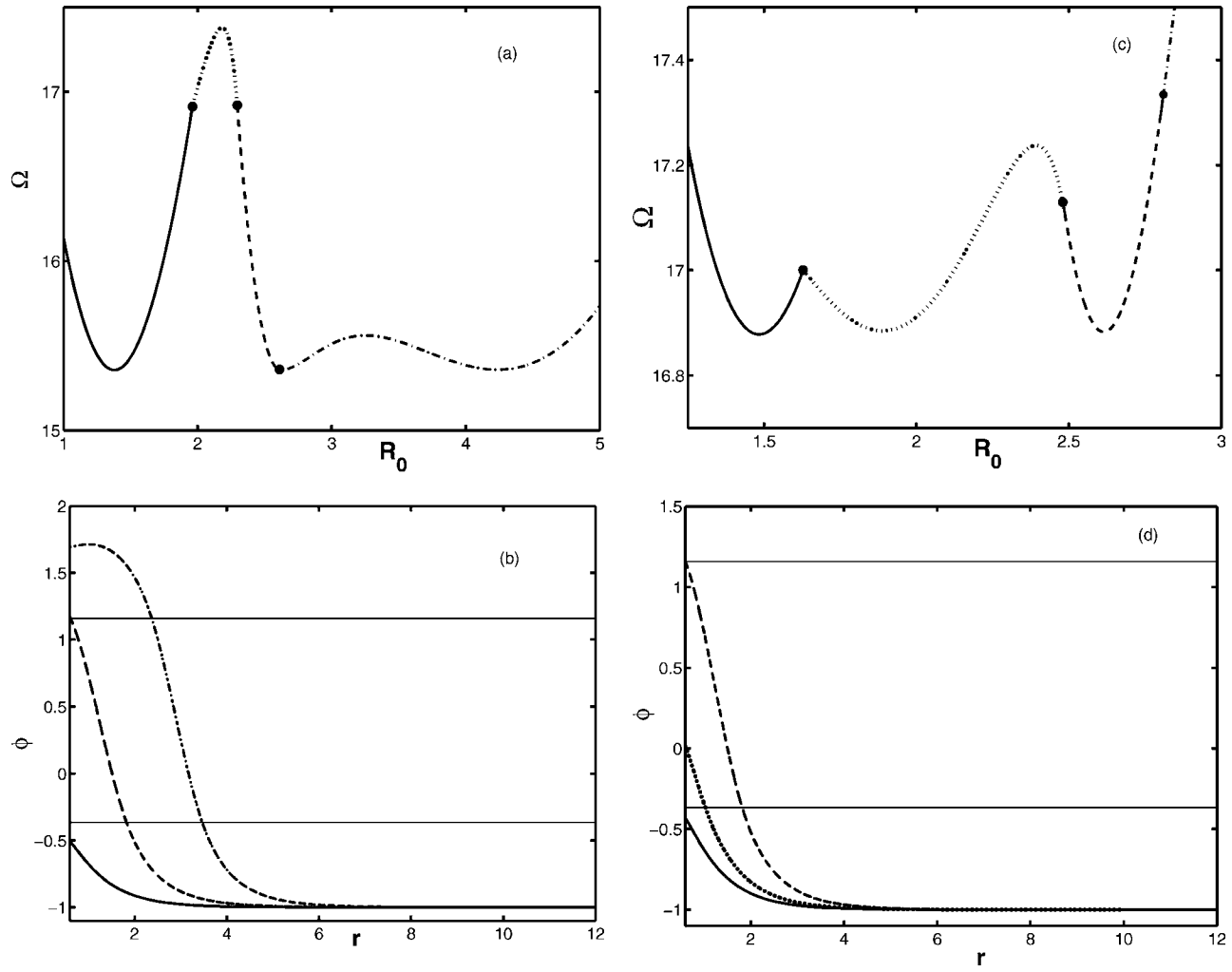

FIG. 9. In (a) interface potential $\Omega[R_0]$ in the triple point located on the left in Fig. 8. The solid line was constructed with what we called the thin 1 interface. The dotted line with profiles named thin 2, the dashed line with the thin 3 profiles, and the dash-dotted line with thick profiles. In (b) we show the three profiles that coexist at this triple point. In (c) we show the interface potential $\Omega[R_0]$ for the surface triple point on the right of Fig. 8 with the same notation as in (a). In (d) the three profiles that coexist at this triple point are shown.

fix the bulk parameters in a region of parameter space, where we know that there are micellarlike metastable states [6]. Here we chose $f_0=1.48$, $B=-4.0$, $A_o=9.2$, $A_a=-9.0$, $\lambda_w=4.0$, and $\lambda_a=1.0$. In this case we can write three possible solutions of the Euler-Lagrange equations. The wall-water interface with the oil phase in contact with the wall, the thick profile, can be written like

$$\phi(r)=\begin{cases}\displaystyle\sum_{i=1}^{4}\frac{A_i}{r}e^{k_{oi}r}+\phi_{bo}, & R<r<R_1,\\ \displaystyle\sum_{i=1}^{4}\frac{B_i}{r}e^{k_{ai}r}, & R_1<r<R_2,\\ \displaystyle\frac{C_1}{r}e^{-k_{w1}r}+\frac{C_2}{r}e^{-k_{w2}r}+\phi_{bw}, & R_2<r<\infty,\end{cases} \tag{18}$$

with two crossing conditions on R_1 and R_2. On the other hand, we calculate the wall-water phase when the middle phase is in contact with the wall, which we call the thin 2 profile; with only one crossing condition in R_2 this is

$$\phi(r)=\begin{cases}\displaystyle\sum_{i=1}^{4}\frac{B_i}{r}e^{k_{ai}r}, & R<r<R_2,\\ \displaystyle\frac{C_1}{r}e^{-k_{w1}r}+\frac{C_2}{r}e^{-k_{w2}r}+\phi_{bw}, & R_2<r<\infty,\end{cases} \tag{19}$$

and the thin 1 profile when the water phase is in contact with the wall,

$$\phi=\frac{C_1}{r}e^{-k_{w1}r}+\frac{C_2}{r}e^{-k_{w2}r}+\phi_{bw}, \quad R_2<r<\infty, \tag{20}$$

where the C_i coefficients are obtained from the wall conditions. Examples of these profiles are shown in Fig. 7 for the same values in the $(\omega_s-\mu_s)$-plane.

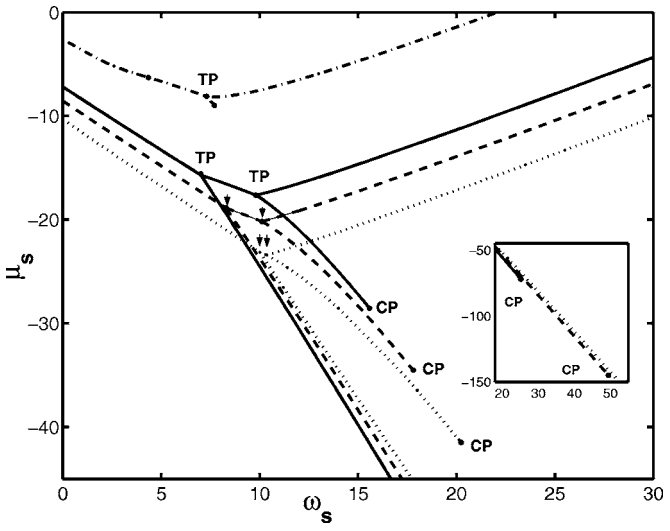

FIG. 10. Details of the behavior of the surface phase diagrams for different radii. The inset shows the behavior of the critical point in the thick—thin-3 coexistence.

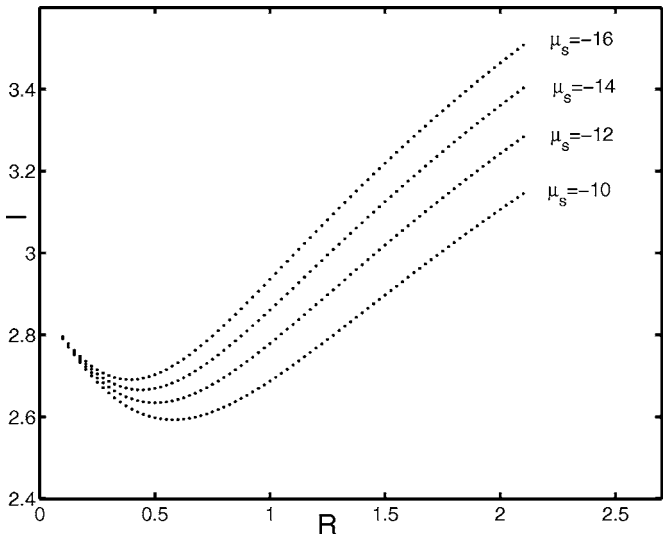

FIG. 11. Thickness of the wetting layer $l=R_1-R$ vs the radius of the sphere R for various values of the surface chemical potential μ_s. The other surface parameters are $\omega_s=0$ and $g_s=6.0$. Notice the minimum that corresponds to a micelle-type structure.

Using profiles generated by Eq. (18), there is again the possibility of a local minimum of the free energy where the value of $\phi(R)=\phi_1$ is fixed at the solid interface, and since, at $r=R=R_1$, there is no need to satisfy the condition on the discontinuity of the third derivative, we drop it. To this we assign the name thin 3 profile. Then, in this case, we must obtain the phase behavior with these four states. First, we consider the profile in the Eq. (18) and we obtain its free energy substituting it in Eq. (1) and, then, we do the same with the profile (20). We compare their energies and we obtain a part of the phase diagram that is a boundary phase separating the stability of the thin-1-thick phases. Then we look for a coexistence between the thick and thin 3 phases. As we approach the critical point of this transition, there is a second solution for Eq. (18) that competes in energy with the thin 3 state and is different from the thick state (we still call this state the thin 3 state). Then the phase coexistence near the critical point of this branch is between two solutions of Eq. (18). There is also a branch, on the phase diagram that separates the thin 1 states from the thin 2 states, and another that separates the thin 2 and thin 3 states, and finally a small branch that separates the thin 1 and thin 3 states. On the convergence of the thick–thin-3, thick–thin-1, and thin-1–thin-3 lines we have a triple point that involves the thick phase. Also on the convergence of the thin-3–thin-2, thin-2–thin-1, and thin-1–thin-3 branches we obtain a second triple point that involves the thin 1 state. In Fig. 8 we show this complex behavior. For clarity, in Fig. 9 we show the interfacial potentials constructed as in Sec. III, with its obvious complications, and we have used $\phi(R_0)=-0.8$. The profiles at the two triple points are shown in Figs. 9(b) and 9(d).

It is interesting to see the evolution of this phase diagram, as we change the radius of the surface; this is shown in Fig. 10. There we see that for large radii there is a single branch that separates the thick and thin 1 states; as the radii are decreased we obtain a critical point (thin-2–thin-3) in equilibrium with the thin 1 state, and then a branch of thin-2–thin-3 coexistence appears and at some R there is equilibrium between a critical point (thick–thin-3) in equilibrium with the thin-1 state (not shown in the figure). As the radius of the surface is decreased further the branch of thick–thin-3 coexistence grows. And at even smaller radii the two triple points merge in a four-state coexistence.

In simple fluids for short-ranged potentials and in the mean field, the thickness of the quasiwetting layer l increases with the radius as $l\approx\xi\ln[CR/(2\sigma\xi)]$, where ξ is the correlation length, σ is the surface tension, and C is a constant [15]. It has been shown [6] that the TPM model includes, besides the usual surface tension, rigidity and spontaneous curvature terms, so we do not expect this simple behavior for the wetting layer as the radius of the spherical surface increases. Instead we find that for small R the wetting layer decreases until some value where there is a minimum for l. For larger values of R the layer wetting grows and the behavior is logarithmic for $R\to\infty$. The reason for this peculiar behavior is that there is an intrinsic micelle structure with radius R_m and the introduction of a solid into it only fills the space formerly occupied by oil. When the radius of the sphere is larger than R_m we recover a behavior close to that of a simple fluid. This is shown in Fig. 11 together with the behavior of R_m with the surface chemical potential.

V. SUMMARY AND DISCUSSIONS

We have calculated several wetting transitions on a spherical wall by amphiphilic mixtures. We used Ginzburg-Landau theory with a piecewise parabolic form for the free energy in bulk. With the TPM model we can find analytical expressions for the density profiles. However, there is a disadvantage pointed out in other work [9], where the usual solutions of the complete set of the Euler-Lagrange equations for the thin profile do not exist. Even with this drawback we can follow the quasiwetting transitions up to their critical point, using local minima of the grand potential. Other short-

comings are the discontinuities in the first derivative of effective potential and in the third derivatives of the profiles. Here we comment that an effective potential was calculated and could be used in renormalization calculations to include fluctuations. In this work we are only interested in the possible local minimal points that give us the phase behavior.

This work with the TPM model could be compared with results of the continuous ϕ^6 model where $f(\phi)=\lambda\phi^2(\phi-\phi_o)^2(\phi-\phi_w)^2$. This latter model has difficulties as the numerical problems involved in obtaining numerical stable profiles. However, we think that the fundamental physics of the problem is well captured by the TPM model. The ϕ^6 model could be richer in other aspects. This speculation is motivated by the work of Upton *et al.* [16], where the transitions obtained from piecewise parabolic form particulary double-parabola model (DPM) are compared with the transitions obtained from the continuous form for the free energy. In the continuous model, two critical points merge at a critical double point; this characteristic is hidden in the DPM model. The equivalent of this comparison is currently under investigation.

We chose two sets of parameters that could be of interest in applications. In the first set we have obtained the properties of a mixture when the uniform microemulsion phase has a structure factor with oscillations that provoke the formation of a corona around the solid particle. It has been shown [20] that in such situations there are forces between two particles that could replace the Coulombic interactions to prevent the coagulation in the production of paints, coatings, foods, and drugs. In the other set we have shown that to coat a particle with a microscopic layer the size of the particle has to be smaller than the size of the swollen micelles that form naturally in the microemulsion. We think that this work will encourage experimental work of the wetting behavior of complex fluids on nanoparticles and colloids [21,22] or the stability of emulsions [23] and that the wetting transition on spheres by these mixtures should be accessible in experiments.

[1] B. K. Paul and S. P. Moulik, Curr. Sci. **80**, 990 (2001).
[2] R. P. Bagwe and K. C. Khilar, Langmuir **16**, 905 (2000).
[3] G. Gompper and M. Schick, in *Phase Transitions and Critical Phenomena*, edited by C. Domb and J. L. Lebowitz (Academic Press, London, 1995), Vol. 16.
[4] G. Gompper and S. Zschocke, Europhys. Lett. **16**, 731 (1991).
[5] C. Varea and A. Robledo, Physica A **290**, 360 (2001).
[6] C. Varea and A. Robledo, Physica A **306**, 301 (2002).
[7] G. Gompper, R. Holyst, and M. Schick, Phys. Rev. A **43**, 3157 (1991).
[8] G. Gompper and S. Zschocke, Phys. Rev. A **46**, 4836 (1992).
[9] F. Clarysse and C. J. Boulter, Physica A **278**, 356 (2000); C. J. Boulter and F. Clarysse, Phys. Rev. E **60**, R2472 (1999).
[10] A. Ciach and V. Babin, J. Mol. Liq. **112**, 37 (2004).
[11] R. Holyst and P. Oswald, J. Chem. Phys. **109**, 11051 (1998).
[12] X. L. Zhou, L. T. Lee, S. H. Chen, and R. Strey, Phys. Rev. A **46**, 6479 (1992).
[13] D. D. Lee, S. H. Chen, C. F. Majkrzak, and S. T. Satija, Phys. Rev. E **52**, R29 (1995).
[14] R. Holyst and A. Poniewierski, Phys. Rev. B **36**, 5628 (1987).
[15] M. P. Gelfand and R. Lipowsky, Phys. Rev. B **36**, 8725 (1987).
[16] P. J. Upton, J. O. Indekeu, and J. M. Yeomans, Phys. Rev. B **40**, 666 (1989).
[17] T. Bieker and S. Dietrich, Physica A **252**, 85 (1998).
[18] D. Beysens and D. Estève, Phys. Rev. Lett. **54**, 2123 (1985).
[19] M. Teubner and R. Strey, J. Chem. Phys. **87**, 3195 (1987).
[20] P. Galatola and J. B. Fournier, Phys. Rev. Lett. **86**, 3915 (2001).
[21] S. R. Kline and E. W. Kaler, J. Colloid Interface Sci. **203**, 392 (1998).
[22] H. Stark, J. Fukuda, and H. Yokoyama, J. Phys.: Condens. Matter **16**, S1911 (2004).
[23] B. P. Binks, J. H. Clint, A. K. F. Dyab, P. D. I. Fletcher, M. Kirkland, and C. P. Whitby, Langmuir **19**, 8888 (2003).